Soft Matter

PAPER

View Article Online
View Journal

Check for updates

Cite this: DOI: 10.1039/d5sm01144b

Softening of shear-thickening in suspensions by the addition of large particles

Alice Pelosse *[a] and Heinrich M. Jaeger[ab]

This study investigates the rheological behavior of shear-thickening suspensions made with different types of small particles upon the addition of much larger particles referred to as granules. The size ratio ranges from 20 to 120. We examine the effects of granule size, volume fraction, and surface properties on shear-thickening characteristics. Starting from a fumed silica suspension exhibiting discontinuous shear thickening (DST), the addition of granules at different volume fractions shifts the onset of thickening to lower shear rates. Concomitantly, the strength of the thickening, quantified by the thickening index, decreases, transitioning from DST to continuous shear thickening (CST). Comparison with suspensions of silica spheres reveals a similar trend, suggesting generality across different systems. These results contrast with the results of prior work on cornstarch-based and nanosilica sphere suspensions, where granule addition was found to enhance thickening. We discuss possible origins of these differences and propose a mechanism for the observed softening: when granules are much larger than the surrounding particles, they induce local variations in shear rate and disrupt the formation of an extended network of force chains. These findings highlight the critical role of particle size ratio in determining the rheology of complex suspensions, paving the way for tailoring material properties for industrial and scientific applications.

Received 14th November 2025,
Accepted 3rd February 2026

DOI: 10.1039/d5sm01144b

rsc.li/soft-matter-journal

Open Access Article. Published on 27 February 2026. Downloaded on 3/21/2026 5:15:28 AM.
This article is licensed under a Creative Commons Attribution 3.0 Unported Licence.

1 Introduction

Shear-thickening of a suspension, *i.e.*, the increase of viscosity with strain rate or applied stress, is observed in a plethora of systems, such as starches, dense colloidal and confined granular suspensions, or suspensions of functionalized particles. This phenomenon usually appears at relatively high particle volume fractions and is thus intrinsically related to the jamming of the solid phase.[1,2]

Several mechanisms can explain such a rheology and contribute in different proportions to an observed shear-thickening behavior,[3] which can result in continuous shear thinning (CST) or discontinuous shear-thickening (DST). The transition from an ordered to a disordered state has been evidenced for highly monodisperse particles while increasing the flow shear rate and is concomitant with an increase in the viscosity.[4,5] This increase can be smooth or very abrupt, but this mechanism cannot be sufficient to account for shear-thickening in most suspensions, where ordering and crystallization do not occur due to particle size variation. Another mechanism leading to shear-thickening is that of hydroclusters, coming from hydrodynamic interactions between the particles through viscous pressure as they are brought close. These hydroclusters are therefore transient aggregates of particles, formed when a sufficiently large shear rate is applied to the system.[6] They grow in size with increasing volume fraction and shear rate (or the Peclet number), correlated with the shear-thickening in the suspension.[7] However, such a mechanism seems to be limited to CST and cannot account for DST.[3] Instead of hydroclusters, physical and chemical friction between the particles in a concentrated suspension is able to create force chains which percolate in the system, resist shear, and can lead to DST rheology of the suspension.[8] Additional complexity arises from the solvent, which mediates hydrodynamic interactions and also specific surface interactions of the particle surfaces.[9] The frictional contribution to dissipation relative to hydrodynamic lubrication depends on the applied shear stress and inter-particle friction and controls the CST/DST behavior of the suspension.[10,11] In particular, strong thickening is correlated with the activation of frictional contacts.[12] This activation creates force chains and whole clusters of frictionally coupled particles, whose size and velocity correlation grow with applied shear.[8,13] This increased dissipation mechanism depends on the friction strength[14] and also on the confinement stress that will trigger DST when a system is frustrated and cannot dilate to rearrange.[15] In addition to increasing friction, particle roughness and asperities can yield particle interlocking, thereby further

[a] James Franck Institute, University of Chicago, Chicago, Illinois 60637, USA. E-mail: alice.pelosse@espci.psl.eu
[b] Department of Physics, The University of Chicago, Chicago, IL 60637, USA

Open Access Article. Published on 27 February 2026. Downloaded on 3/21/2026 5:15:28 AM.
This article is licensed under a Creative Commons Attribution 3.0 Unported Licence.

decreasing both the shear rate and the particle volume fraction required to turn on shear-thickening.[16,17]

Non-Brownian cornstarch suspensions have been extensively studied and exhibit strong DST at relatively low volume fraction. Brownian suspensions of nanoparticles can be shear-thickening depending on the nature and strength of the aforementioned frictional effects. In particular, fumed silica nanoparticles, which are aggregates of silica nanospheres and have fractal-like shapes of size ranging from 100 to 500 nm, can exhibit strong DST.[18,19] Suspensions of non-aggregated silica nanospheres in appropriate solvents can also exhibit CST/DST behavior.[20] Simulations suggest that thermal effects should mainly shift the shear-thickening onset to higher values, with Brownian forces adding to repulsive interactions between the particles.[21,22]

In this article, we investigate how the addition of large particles, here termed granules, affects the shear-thickening of a colloidal suspension effectively playing the role of a non-Newtonian solvent. The granule concentration was chosen such that these larger particles, by themselves, do not exhibit any thickening or thinning. The addition of these granules to a non-Newtonian solvent is relevant for many industrial processes (concrete) and natural systems (blood) and raises non-trivial questions. In the low-inertia regime, the viscosity of a suspension made solely with these granules is relatively simple when the suspending fluid is Newtonian. In that case, the viscosity of the suspension is proportional to the suspending fluid viscosity, and the relative viscosity of the suspension to the fluid solvent, η_r, is solely a function of the granule volume fraction, ϕ_G, normalized by the jamming fraction, ϕ_G^c, which depends on the particle properties.[23] In particular, the relative viscosity of granular suspensions with different polydispersity[7,24,25] and surface roughness[26] can be collapsed onto the same master curve, which diverges as jamming is approached, *i.e.* as $\phi_G/\phi_G^c \rightarrow 1$. This geometrical effect of polydispersity saturates for large size ratios, typically larger than ten,[24] with a milder and milder increase in the jamming volume fraction for increasing size ratio.[27,28]

For very large size ratios, *e.g.* granules in a colloidal suspension, the granule environment can be approximated by a continuous phase with a non-Newtonian viscosity.[29] In that situation, adding granules to the non-Newtonian fluid should increase the zero-shear viscosity by a factor close to the relative viscosity, η_r. However, adding granules to this solvent raises questions about the relevant shear rate, which now becomes locally enhanced. This enhanced shear rate is captured by a lever function and depends on the granule volume fraction only.[23,30]

Experiments where larger granules were added to a non-Brownian, shear-thickening cornstarch suspension have reported both effects, namely (i) the increase in the zero-shear viscosity and (ii) the shift of the onset of shear thickening to smaller shear rates.[31] Importantly, in these systems, a transition from CST to DST behavior was observed. In other words, the shear-thickening was enhanced. This was explained as a wall-effect, whereby volume exclusion near the surface of the large granules locally increased the volume fraction of the surrounding shear thickening suspension, resulting in increased dissipation of the interstitial fluid.[32] The latter is thus a finite size effect arising when the granule size is larger, but still close to that of the particles in the suspending fluid.

Here, we discuss what happens for even larger size ratios, ranging from 20 to 120, between micron-size granules and nanoparticles. We show that in this limit, we obtain similar results for the critical shear rate and shear stress to obtain shear-thickening, but find opposite behavior for the strength of the shear-thickening upon addition of granules. Specifically, instead of enhanced shear thickening we find a transition from DST to weaker, CST behavior when adding granules. Interestingly, the granule size still matters despite the large size contrast in our systems.

This article is organized as follows. In the next section (Section 2), we present the different suspensions and protocols we used in our experiments. The results are described in Section 3. A discussion and comparison with other systems found in the literature is then presented in Section 4, and a model to account for our observations is drawn, before we conclude.

2 Materials and methods

2.1 Shear thickening suspensions

Hydrophilic fumed silica particles (AEROSIL OX50, ρ_p = 2.2 g cm^{-1}) were dispersed in liquid PEG (M_w = 200 g mol^{-1}, ρ_f = 1.12 g cm^{-3}, and η_f = 57 mPa s measured at 22 °C) purchased from Sigma Aldrich. To ensure homogeneous dispersion, the fluid was weighed, and the desired amount of particles was added progressively in three steps. After each addition, the mixture was subjected to sonication, followed by manual and mechanical mixing. The final suspension was further sonicated and mixed using a roller device for one week, ensuring it reached a stable state.

Spherical colloidal silica suspensions were prepared following the same protocol, using particles with a diameter of approximately 500 nm, 1000 nm, and 2000 nm (Angstrom-Sphere, ρ_p = 1.8 g cm^{-3}) in the same PEG solvent. Similarly, an extended mixing period of one week, with regular sonication steps, was required to obtain a uniform dispersion of particles. Extending the mixing time beyond this, up to one month, had no measurable effect on the suspension rheology.

The nanoparticle volume fraction of the shear-thickening suspension is defined as the concentration excluding intruding particles, $\phi_{STF} = V_{NP}/(V_{NP} + V_f)$, where V_{NP} and V_f denote the volumes of nanoparticles and fluid, respectively. Note that, under this definition, ϕ_{STF} represents the concentration within the interstitial fluid and not in the total suspension after the introduction of larger intruding particles. The nanoparticle volume fraction, and thus their proportion within the solid phase, decreases upon addition of granules. This is illustrated for the fumed silica suspensions at ϕ_{STF} = 30% in Table 1, and for the silica spheres at ϕ_{STF} = 51% in Table SM1 of the SI.

 This journal is © The Royal Society of Chemistry 2026

Open Access Article. Published on 27 February 2026. Downloaded on 3/21/2026 5:15:28 AM.
This article is licensed under a Creative Commons Attribution 3.0 Unported Licence.

Table 1 Volume fractions in a system where granules have been added to a nanoparticle suspension with an initial solid fraction, ϕ_{STF}, of 30%

Granule volume fraction ϕ_G (%)	0	20	30	40	45
Volume fraction occupied by nanoparticles (%)	30	24	21	18	17
Total volume fraction of solids (%) ϕ_{total}	30	44	51	58	62
Proportion of nanoparticles in total volume of solids α (%)	100	54	41	31	27

2.2 Granules

Large particles, referred to as granules, were selected to test various properties, including size, density, and surface characteristics. The granules used included hollow glass spheres with significant polydispersity (Supelco, Sigma-Aldrich, ρ_G = 1.0 g cm^{-3}, 9–13 μm), monodisperse PMMA spheres (CA20 and CA60, Microbeads, ρ_G = 1.2 g cm^{-3}, (20 ± 1) μm and (60 ± 2) μm), monodisperse polystyrene spheres (TS20, Microbeads, ρ_G = 1.1 g cm^{-3}, (20 ± 3) μm) and monodisperse glass spheres (Soda Lime Solid Glass Microspheres, Cospheric, ρ_G = 2.5 g cm^{-3}, 53–63 μm). These granules were added to the shear-thickening suspension at volume fractions ranging from 20% to 45%. The granule volume fraction, ϕ_G, is defined as the ratio of the granule volume to the total suspension volume, $\phi_G = V_G/(V_G + V_{STF})$, where V_G is the granule volume, and V_{STF} is the volume of the shear-thickening suspension. These particles in Newtonian PEG-200 do not shear-thicken, and exhibit a Newtonian behavior and/or a shear-thinning behavior at high shear rate, as expected for such suspensions of non-Brownian particles, see Fig. SM1 of the SI.

2.3 Rheology protocol

Rheological measurements were conducted using a stress-controlled rheometer (Anton Paar, MCR301) with a 25-mm plate–plate geometry, maintained at a controlled temperature of 22 °C. To prevent slippage when measuring samples containing the largest granules, sandpaper was taped on the plates. The gap height was set to be at least 10 times larger than the size of the largest particles, typically ranging from 0.5 to 1 mm. Prior to measurements, suspensions were pre-sheared at a stress of 1 Pa for 60 s. Subsequently, they were subjected to an upward and downward stress ramp, typically ranging from 1 Pa to 1000–10 000 Pa and 30 s per point. Upward and downward ramps produced identical results. For samples with high granule volume fractions, experiments were stopped at lower shear stress to avoid suspension ejection. Good reproducibility was observed, with consistent results across different samples (typically three).

3 Results

3.1 Shear-thickening fluids without granules

In Fig. 1(a) and (b), the steady shear viscosity of a fumed silica suspension is plotted as a function of the shear rate and shear stress for different volume fractions, ranging from ϕ_{STF} = 10% to ϕ_{STF} = 30%. For the highest volume fraction, ϕ_{STF} = 30%, the suspension exhibits a discontinuous increase in viscosity at a critical shear rate $\dot{\gamma}_{c,0}$ = 50 s^{-1} and at a critical stress σ_c = 40 Pa. This discontinuous behavior is also captured by the log–log slope of the viscosity *versus* shear stress, defined as $\beta = \mathrm{d}\ln(\eta)/\mathrm{d}\ln(\sigma) = \dot{\gamma}(\mathrm{d}\eta/\mathrm{d}\sigma)$ (see Fig. 1(c)). This parameter, referred to as the thickening index, is negative in the shear-thinning regime, zero for Newtonian fluids, and positive for shear-thickening fluids. In the case of discontinuous shear thickening (DST), $\beta \to 1$.

For all volume fractions, β is negative at low shear stress, corresponding to the shear-thinning behavior observed in Fig. 1(a). The thickening index then becomes positive as shear stress/rate are increased. For the highest concentration, ϕ_{STF} = 30%, β changes sign at σ_c = 40 Pa and plateaus at β = 1 over a large range of shear stress, see Fig. 1(b) and (c). At lower fumed silica concentrations, the shear thickening is less pronounced, as evidenced by the thickening index, which does not reach unity (Fig. 1(b) and (c)). For these suspensions, a point of

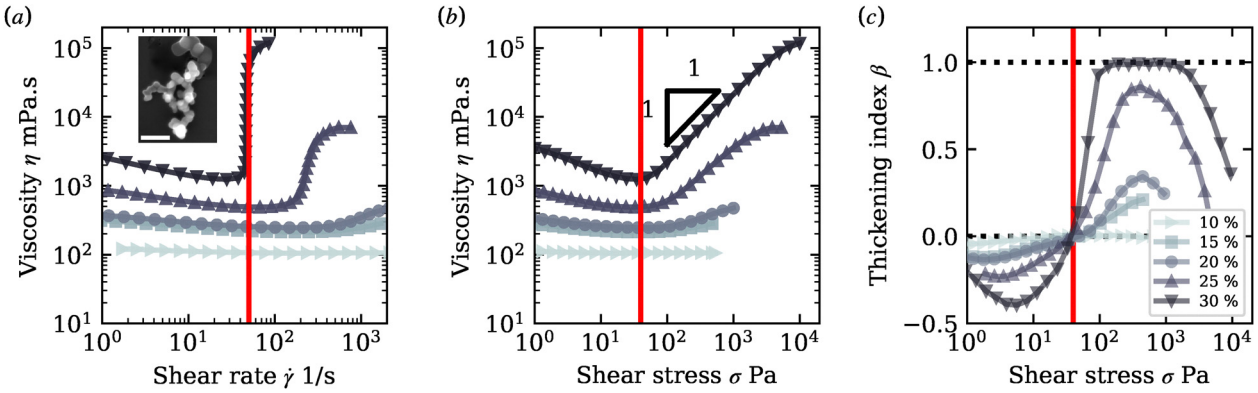

Fig. 1 Steady shear rheology of fumed silica suspensions in PEG200 for various volume fractions, ranging from ϕ_{STF} = 10% to 30%. (a) Viscosity as a function of shear rate. (b) Viscosity as a function of shear stress. (c) Thickening index as a function of shear stress. Red vertical lines indicate the onset of discontinuous shear thickening (DST) for the most concentrated suspension, with ϕ_{STF} = 30%.

Open Access Article. Published on 27 February 2026. Downloaded on 3/21/2026 5:15:28 AM.
This article is licensed under a Creative Commons Attribution 3.0 Unported Licence.

maximum thickening can be identified, characterized by a shear rate $\dot{\gamma}_{max}$, a shear stress σ_{max}, and a thickening index β_{max}. In the case of DST, $\dot{\gamma}_{max} = \dot{\gamma}_c$, $\sigma_{max} = \sigma_c$, and $\beta_{max} = 1$.

3.2 DST fluids and 20-μm granules

We now turn to mixtures of shear-thickening suspensions with large granules, with variable granule size, concentration, and surface properties. Note that these particles, up to the concentrations used here, do not shear-thicken in a Newtonian solvent and exhibit a Newtonian behavior, as shown in Fig. 2(a).

In Fig. 2(b), the viscosity of suspensions containing varying amounts of 20 μm PS and PMMA spheres is plotted as a function of the shear rate. The suspending fluid is a shear-thickening suspension of fumed silica at a volume fraction ϕ_{STF} = 30%. At this particle size, the density of the granules does not significantly affect the suspension behavior, as evidenced by the good overlap of the PS and PMMA rheology data for granule volume fractions ϕ_G = 20% and 40%.

As the granule fraction increases from ϕ_G = 20% to ϕ_G = 45%, two trends are observed in Fig. 2(b): (i) the low-shear viscosity increases, which is expected due to the additional granule loading. This behavior is consistent with the scaling of non-Brownian suspensions, where the viscosity is the product of the suspending fluid viscosity and the suspension's relative viscosity, η_r, that can be extracted from Fig. 2(a). (ii) The shear rate corresponding to the onset of shear thickening decreases with increasing ϕ_G, shifting the viscosity curves toward lower shear rates. This shift arises from local effects: the granules amplify the local shear rate in the interstitial fluid, triggering shear thickening at smaller applied shear rates, $\dot{\gamma}_c(d_G,\phi_G)$. Shifting the low-shear suspending fluid viscosity by $\dot{\gamma}_c(d,\phi_G)$ along the x-axis and multiplying it by the relative viscosity $\eta_r(\phi_G)$ along the y-axis shows a good collapse in the shear thinning regime, see the blue curves in Fig. 2(b).

A third observation is the softening of the shear thickening as the granule loading increases. This softening is reflected in the slope of the viscosity curves plotted as a function of shear rate in Fig. 2(b), or as a function of shear stress in Fig. SM2 of the SI. The latter point is not trivial and in contradiction with previous results obtained in a different shear-thickening fluid.[31–33] To best quantify the softening in thickening, the thickening index and the different suspensions are plotted in Fig. 2(c). While the suspensions exhibit similar rheological behavior in the shear-thinning regime ($\beta < 0$), the thickening index decreases with increasing granule content in the shear-thickening regime ($\beta > 0$). The effect of granules on β seems to appear right after the shear-thickening onset. At ϕ_G = 20%, the suspension nearly exhibits discontinuous shear thickening (DST) with $\beta_{max} \approx 1$. The thickening is however mildly weakened considering that a higher shear stress is required to reach this value. At higher granule fractions, the thickening transitions to a continuous shear-thickening (CST) regime with $\beta_{max} < 1$.

Finally, the shear stress at the onset thickening, $\sigma_c \simeq 40$ Pa, measured for $\beta = 0$, seems to be fixed at the critical shear stress of the pure fumed silica suspension (within experimental uncertainty), see Fig. 1(b) and 2(c), in contrast to the critical shear rate which decreases with increasing ϕ_G, see Fig. 2(b).

3.3 DST fluids and other granules

The effects of granule size, polydispersity, and surface properties are now investigated using larger PMMA spheres and smaller, polydisperse glass spheres. In the same fumed silica suspension as used in Fig. 2(b) and (c), monodisperse 60 μm and polydisperse 10 μm spheres are combined, and their rheology are shown in Fig. 3(a) and (b), respectively. The volume fraction of the granules, ϕ_G, is varied over the same range as in Fig. 2. Similar trends are observed in both cases, as shown by the thickening index plotted against shear stress (main graphs) and the viscosity curves as a function of shear rate (insets). The viscosity curves plotted as a function of shear stress are also shown in Fig. SM2 of the SI. Again, the

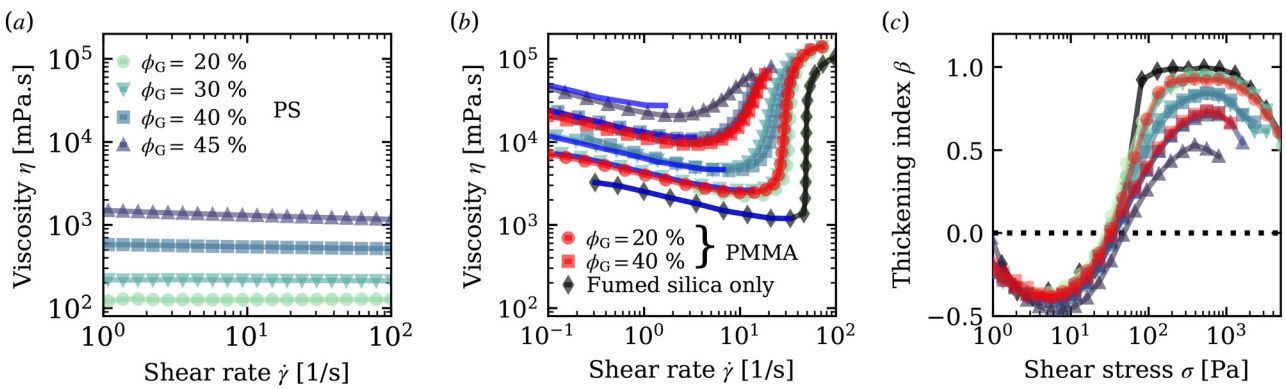

Fig. 2 Steady shear rheology of suspension made with 20 μm PS spheres (a) in PEG200, and (b) in a fumed silica suspension in PEG200 (ϕ_{STF} = 30%), for granule volume fractions ranging from ϕ_G = 20% to ϕ_G = 45%. Main graph: viscosity as a function of shear rate. Relative viscosity $\eta_r = \eta/\eta_f$ for increasing granule volume fractions: 2.2, 3.8, 9.6, 23. (b) Blue lines represent the low-shear viscosity prediction based on the relative viscosity of granular suspensions, η_r, measured in (a), with the shear rate shifted to align with the onset of shear thickening. Red curves correspond to suspensions prepared using 20 μm PMMA spheres instead of PS. Black curves represent the baseline behavior of the pure fumed silica suspension extracted from Fig. 1 at ϕ_{STF} = 30%. (c) Thickening index as a function of shear stress.

 This journal is © The Royal Society of Chemistry 2026

Open Access Article. Published on 27 February 2026. Downloaded on 3/21/2026 5:15:28 AM.
This article is licensed under a Creative Commons Attribution 3.0 Unported Licence.

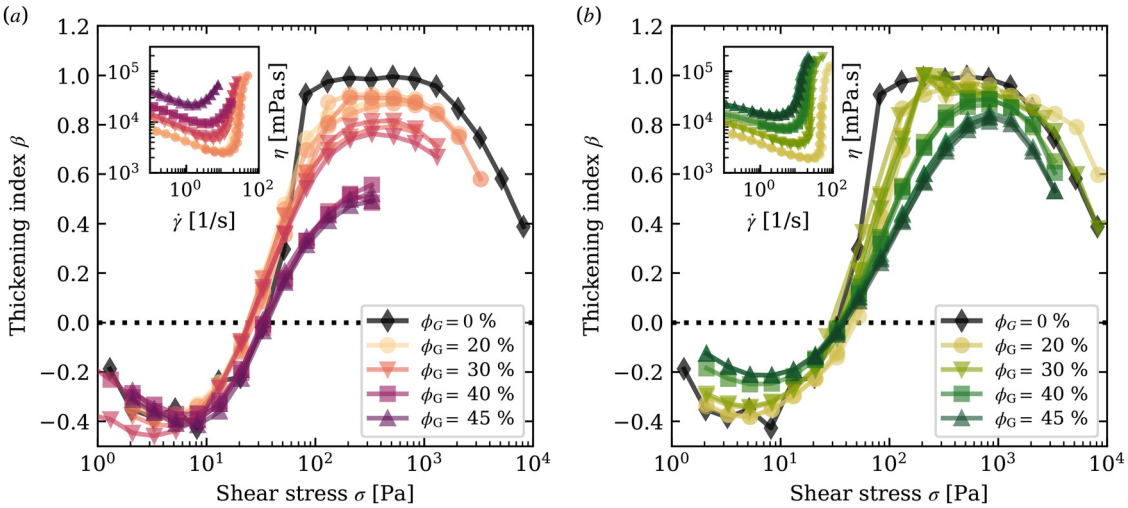

Fig. 3 Steady shear rheology of suspension made with a fumed silica suspension in PEG200, ϕ_{STF} = 30% combined with (a) 60 μm PMMA spheres, and (b) 10 μm glass spheres, for granule volume fractions ranging from ϕ_G = 20% to ϕ_G = 45%. Main graphs: thickening index as a function of the shear stress. Insets: viscosity as a function of shear rate. Black curves represent the baseline behavior of the pure fumed silica suspension extracted from Fig. 1 at ϕ_{STF} = 30%.

shear rate at the onset of shear thickening decreases with increasing granule volume fraction, consistent with the results obtained with the 20 μm PS spheres. Also, the shear stress at the onset of shear thickening, σ_c (defined as the stress where β = 0), remains nearly constant regardless of the granule size and volume fraction, as evidenced in the main panels of Fig. 3. From this figure, it also appears that for a given granule volume fraction, larger granules lead to a stronger softening of the shear-thickening, as evidenced by the smaller values of β with the 60 μm particles. These results further confirm the generality of the trends observed with different granule types and sizes.

The shear-thickening characteristics for different granule sizes and granule volume fractions in the same fumed silica suspension are summarized in Fig. 4. In Fig. 4(a), the shear rate at the onset of shear thickening, $\dot{\gamma}_c$, is plotted as a function of the granule volume fraction, ϕ_G. The data confirm that higher granule volume fractions result in earlier shear-thickening onset. Additionally, this figure highlights the influence of the granule size: larger granules lead to a greater shift in the effective shear rate. These differences between fumed silica-based and cornstarch-based systems are explored further in the discussion section.

Fig. 4(b) presents the maximum thickening index, β_{max}, for the various suspensions. The trend confirms our earlier observations in Fig. 3: shear thickening becomes weaker as the granule volume fraction increases and the softening is more pronounced as the granule size increases.

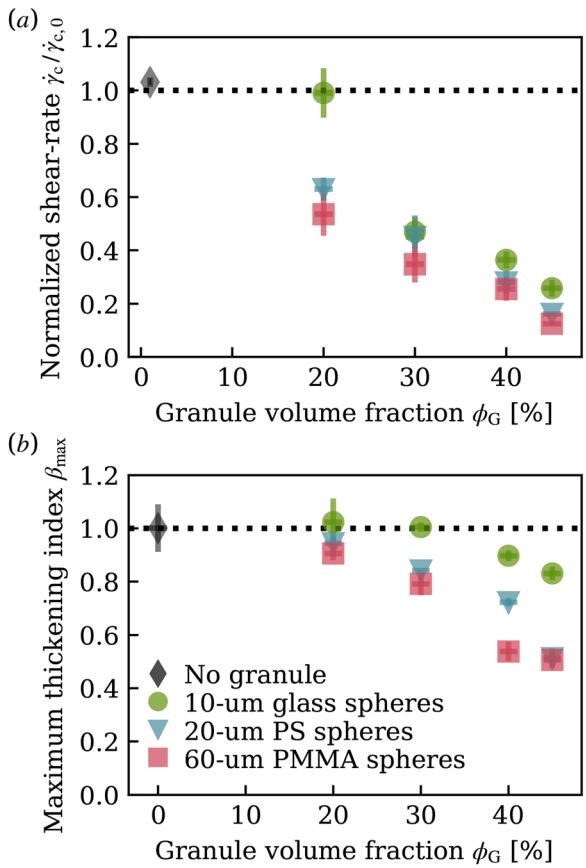

Fig. 4 Summary of the shear thickening features of a mixture of a DST suspension of fumed silica ϕ_{STF} = 30%, with larger granules (see legend). (a) Shear rate at the onset of thickening behavior and (b) maximum thickening index.

3.4 CST fluids and granules

The same trends are observed when 20 μm PS spheres are added to continuously shear-thickening (CST) suspensions of fumed silica, for the volume fraction ranging from ϕ_{STF} = 14% to ϕ_{STF} = 26%, see Fig. 5(a). Note that ϕ_{STF} is defined as the fumed silica volume fraction in the suspending liquid, *i.e.*, as the fumed silica volume fraction in the interstices between the granules. Similarly to the situation with a DST

Open Access Article. Published on 27 February 2026. Downloaded on 3/21/2026 5:15:28 AM.
This article is licensed under a Creative Commons Attribution 3.0 Unported Licence.

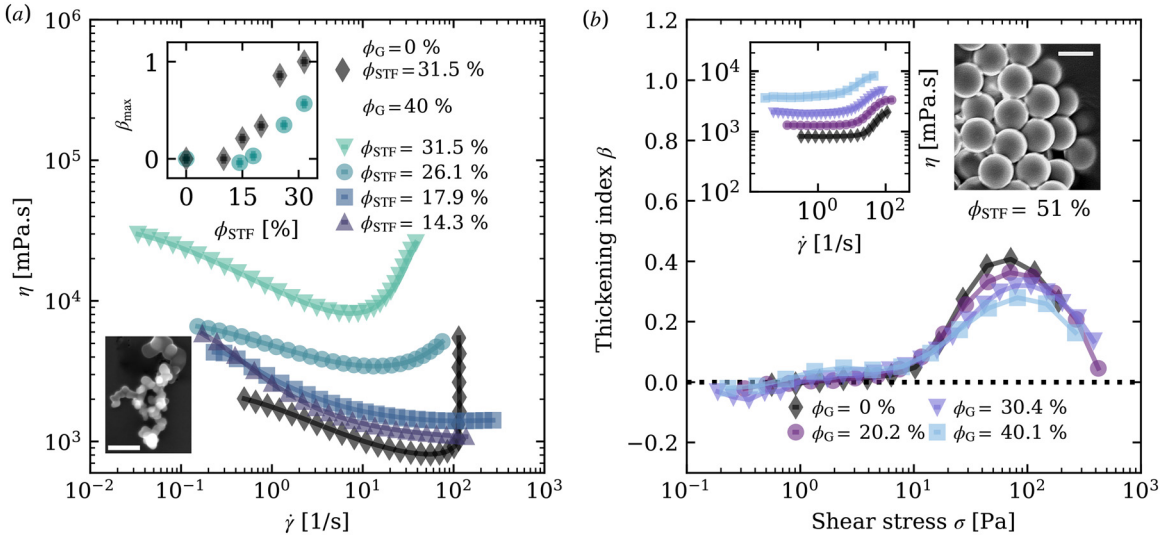

Fig. 5 (a) Rheology of suspensions made with 20 μm PS spheres at ϕ_G = 40%, added in fumed silica (bottom left SEM picture, scale: 200 nm) in PEG200. The volume fraction of the colloids in the suspending medium is varied from ϕ_{STF} = 14.3% to ϕ_{STF} = 31.5%, see the legend. A suspension at ϕ_{STF} = 31.5% with no granule is plotted in black. Inset: maximum thickening index as a function of the fumed silica volume fraction in the suspending fluid without granules (black lozenges) and with 20 μm PS spheres at ϕ_G = 40% (blue circles). (b) Rheology of suspension made with 1 μm colloidal silica spheres in PEG200, ϕ_{STF} = 51% combined with 60 μm PMMA spheres, for granule volume fractions ranging from ϕ_G = 20% to ϕ_G = 40%. Main graphs: thickening index as a function of shear-stress. Insets: steady shear viscosity as a function of shear-rate.

suspension of fumed silica, the strength of the shear-thickening in these CST suspensions, quantified by β_{max} and plotted in the inset of Fig. 5(a), decreases after addition of the granules at ϕ_G = 40%.

To test the generality of the results found with fumed silica, we also investigated shear-thickening fluids made of 500 nm, 1 μm, and 2 μm silica spheres in PEG200 with ϕ_{STF} = 51–52%, and granule volume fraction ranges of ϕ_G = 20–40%, see Table SM1 in the SI. For the dense suspension made with 1 μm silica spheres, and similarly to the low concentration fumed silica suspensions, the baseline viscosity exhibits CST, as shown in Fig. 5(b). The maximum thickening index of this suspension is β_{max} = 0.41. In Fig. 5(b), the thickening index (main graph) and viscosity (inset) upon addition of 60 μm PMMA granules in this suspension are presented for different granule volume fractions. Again, the thickening index decreases with increasing ϕ_G, with for instance β_{max} = 0.28 at ϕ_G = 40%. Moreover, the onset stress for shear thickening, around 10 Pa, remains essentially unchanged upon addition of the large particles. The same trends are observed with the two other dense suspensions of 500 nm and 2 μm silica spheres, see Fig. SM3 in the SI.

These experiments with CST suspensions made of rough, non-spherical fumed silica and smooth silica nano- and micro-spheres thus show trends similar to those found in DST fumed silica suspension, namely (i) an increase of the zero-shear viscosity, (ii) an onset of shear-thickening at smaller shear rates, and (iii) a milder shear-thickening. The latter is seen by the decrease in the maximum value of the thickening index in the insets of Fig. 5(a) and (b). Similar results are seen at higher volume fractions of silica nanospheres.

4 Discussion

In general, for suspensions with a bimodal particle size distribution of small and large particles we can expect that the rheology transitions from the behavior of the small to that of the large particles alone, as the proportion of small particles in the solid phase, α, decreases at fixed total solid volume fraction.[34,35] When adding granules to a suspension of small particles, α decreases, but the total solid volume fraction also increases. In such experiments, in the non-shear-thickening regime of the flow curves, *i.e.* below the critical shear stress, the role of the granules merely is to shift the suspension viscosity upward.[29] In the shear-thickening regime, the onset stress scales inversely with the particle size d according to $\sigma_c \propto d^{-\gamma}$ with exponent γ in the range 1.75 to 3.[34,36–38] We thus expect σ_c to shift to lower values as soon as the large particles contribute significantly to the thickening, provided they do. In our experiments the fraction of granules was varied from ϕ_G = 0% up to ϕ_G = 45%, in which case nanoparticles represent only a quarter of the total solid volume (α = 27%, see Table 1). The finding that σ_c is not varying with the relative proportion of small to large particles for α ranging from 100% to 27% in Fig. 2(c), 3(a), (b), and 5(b), therefore indicates that only the small nanoparticles trigger shear-thickening. That we do not observe a noticeable lowering of σ_c even for α = 27% differs from recent simulations of binary non-Brownian suspensions,[35] where the onset stress decreases from that of a suspension made of only small particles once $\alpha \leq 0.5$. To conclude, this fixed value of σ_c varying d_G and ϕ_G strongly suggests that in all of these systems, granule contribution to the shear-thickening process is negligible in comparison to that of the small particles.

The softening of the shear thickening we observe when granules are added differs significantly from that reported in

 This journal is © The Royal Society of Chemistry 2026

Open Access Article. Published on 27 February 2026. Downloaded on 3/21/2026 5:15:28 AM. This article is licensed under a Creative Commons Attribution 3.0 Unported Licence.

the literature for cornstarch suspensions:[31,32] there, granule addition enhances the shear-thickening behavior and drives a transition from CST to DST for a moderate size ratio between the granules and the cornstarch particles. Madraki *et al.*[32] explained their observed enhancement of shear thickening by an effective increase in the volume fraction of the small particles from ϕ_{STF} to $\phi_{STF,eff}$ due to the presence of the granules. When the size ratio between granules and shear-thickening small particles is not very large, excluded volume near the surface of the granules prevents small particles from packing at their bulk density. This geometric 'wall effect' enhances the effective concentration in the interstitial fluid according to $\phi_{STF,eff}/\phi_{STF} = V_{total}/(V_{total} - V_{shell}) \sim 1 + V_{shell}/V_{total}$, where V_{shell} is the excluded volume of the shell around the granules that depends as $V_{shell}/V_{total} = \phi_G[(1 + d_{STF}/d_G)^3 - 1] \sim 3\phi_G d_{STF}/d_G$ on the diameters of the shear-thickening particles, d_{STF}, and the granules, d_G. In the experiments by Madraki *et al.*,[32] the granules were no larger than 10 times the size of the cornstarch particles (typically 20 μm), so that an appreciable enhancement $\phi_{STF,eff}/\phi_{STF} > 1$ due to the wall effect could be observed. However, in our experiments the characteristic size of the shear-thickening fumed silica particles is 500 nm and the smallest granules are 10 μm such that $d_{STF}/d_G \leq 0.05$, $V_{shell}/V_{total} \ll 1$ and $\phi_{STF,eff}/\phi_{STF} \simeq 1$. Therefore, the wall effect cannot affect the shear thickening propensity in our experiments.

A weakening of the shear-thickening in bimodal suspensions was found in simulations of non-Brownian particles when the total solid volume fraction was kept fixed and small particles were replaced by an equal volume of large ones, *i.e.* for fixed ϕ_{total} and decreasing α.[35,39] For these small size ratios (up to 10), this weakening of the shear-thickening is explained by an increased distance to the jamming volume fraction with bimodal systems. However, for large size ratios, the dependence of the jamming volume fraction on the size ratio saturates. For instance, in a bimodal packing of solid spheres that each individually jam at 60%, the jamming volume fraction increases by up to ≈23% when the size ratio increases from 1 to 20, but only by up to ≈1% when the size ratio increases from 20 to 120, according to the Stovall model.[27] Such an effect could contribute partially to the large variations of β_{max} relative to d_G, observed in Fig. 4(b). However, it is unlikely that the decrease in β_{max} can be explained fully by an increase in the distance to the jamming volume fraction.

An experimental system conceptually close to the one explored here was investigated by Cwalina and Wagner.[33] In their work, the addition of 10 μm polydisperse hollow glass beads to a suspension of 260-nm silica nanospheres led to a strengthening of the continuous shear thickening (CST) response. Specifically, a base suspension at ϕ_{STF} = 40% displayed a thickening index β_{max} = 0.28, which increased to β_{max} = 0.45 upon incorporation of the granular phase at ϕ_G = 45%. This behavior is therefore opposite to that observed in the present systems, where the addition of granules systematically results in a softening of the rheological response, both for fumed silica and for suspensions of monodisperse silica spheres, see Fig. 4(b) and 5(b), respectively. Despite several apparent similarities between the two studies, including the solvent, the particle size range, and comparable preparation and rheological protocols, such a difference in the trend suggests that subtle yet crucial physical parameters may govern the coupling between colloidal and granular phases. One possible explanation could lie in the smaller nanoparticle size used by Cwalina and Wagner,[33] which may enhance the role of colloidal forces. Alternatively, the specific silica nanoparticles or glass beads employed in their study could alter the local stress transmission pathways, thereby favoring a reinforcement rather than a disruption of the force-chain network setting the magnitude of the shear-thickening. Indeed, the apparent decrease in the shear-thickening onset stress, σ_c, upon addition of large particles in their system would indicate that these particles participate in the force chain network of the small particles. In all our systems, however, the onset stress remains independent of both the presence and the concentration of granules, suggesting that the granules do not contribute to the force-bearing network. Also, the viscosity dependency on the gap size, and the negative values of the first normal stress difference N_1 during shear-thickening in Cwalina and Wagner's system suggest strong effects of the hydrodynamics in the shear-thickening process. In the present study, by contrast, the shear-thickening would be stemming from strong frictional contact between the small particles: the fumed silica suspensions are found to have a viscosity independent of the gap size (see Fig. SM4 of the SI), and a positive N_1 (see Fig. SM5 of the SI), in agreement with previous works of Bourrianne *et al.*[19] The consistency of the softening behavior for the different bimodal suspensions, and across a range of particle types, sizes and densities, supports a scenario where addition of granules softens the shear-thickening arising from frictional interactions. Overall, these two sets of observations likely correspond to distinct physical regimes, hydrodynamic and frictional, of the same general phenomenon, in which the interplay between microstructure and stress propagation determines whether the granules disrupt or reinforce the shear-thickening network. More experimental or numerical studies are necessary to enable a unified understanding of the rheology of multiscale suspensions.

One key question thus remains: how can the granule size leave such a clear signature in the rheological behavior of the suspension considering that any granule is much larger than the particles of the shear-thickening suspensions? In particular, why does the strength of shear thickening decrease, and why is the decrease more pronounced as the granule size increases? As mentioned earlier, the addition of granules increases the low-shear viscosity by a factor of $\eta_r(\phi_G)$, which is independent of the granule size. Additionally, and more importantly for shear thickening, it leads to a local enhancement of the shear rate experienced by the small particles within the interstices among the granules. On average, this local enhancement is quantified by the lever function, $\mathscr{F}(\phi_G)$, such that $\dot{\gamma}_{local}/\dot{\gamma}_{macro} = \mathscr{F}(\phi_G)$. Notably, this average enhancement is independent of the granule size. Unlike a pure monomodal

Open Access Article. Published on 27 February 2026. Downloaded on 3/21/2026 5:15:28 AM.
This article is licensed under a Creative Commons Attribution 3.0 Unported Licence.

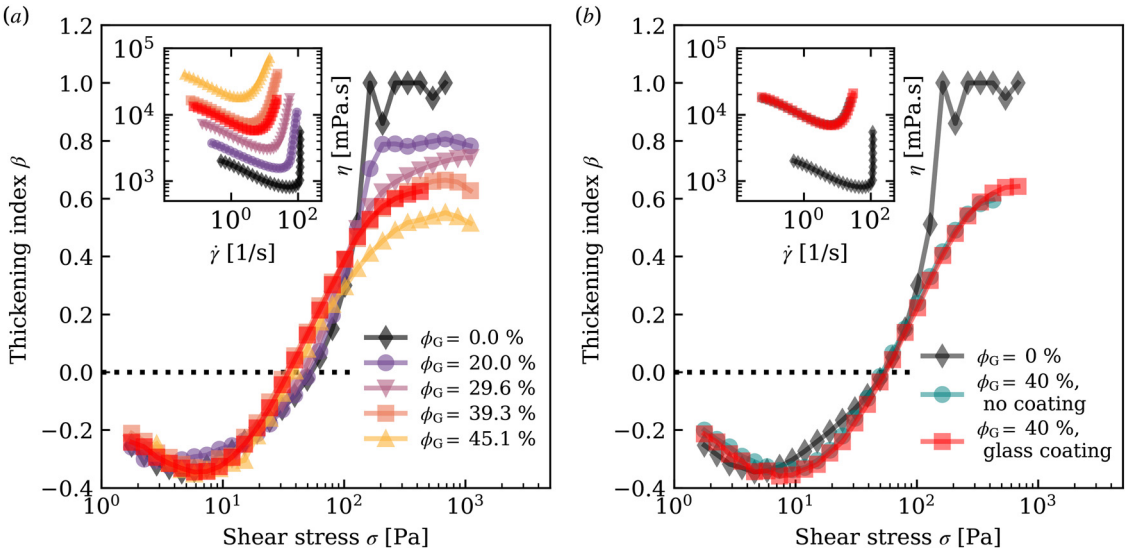

Fig. 6 Steady shear rheology of suspension made with a fumed silica suspension in PEG200, ϕ_{STF} = 30% combined with (a) 60 μm glass spheres for granule volume fractions ranging from ϕ_G = 20% to ϕ_G = 45% and 60 μm PMMA spheres at ϕ_G = 39.9% (red), and (b) 20 μm PS spheres, without and with glass coating at ϕ_G = 40%. Main graphs: thickening index as a function of the shear stress. Insets: viscosity as a function of shear rate. Black curves represent the baseline behavior of a pure fumed silica suspension extracted at ϕ_{STF} = 30%.

suspension sheared uniformly by the walls of a rheometer, this local shear rate within the highly bimodal suspension is non-homogeneous and fluctuates due to granule motion. This heterogeneity in the shear rate could partially explain the observed softening, as it gives rise to localized thickening events across the suspension at a given macroscopic shear rate. However, the behavior of local shear-rate fluctuations is expected to mirror that of the mean local shear rate $\dot{\gamma}_{local}$, which is independent of the granule size and thus does not capture the granule size dependent trends we see in Fig. 4(b).

We thus propose a tentative scenario based on comparing the size of the largest frictionally interacting nanoparticle cluster, $d_{cluster}$, to that of the granules, d_G, to account for the granule size effect. In suspensions made of small particles only, $d_{cluster}$ is a sole function of $\dot{\gamma}_{local}$ and friction coefficient. In this scenario, and in the presence of large intruders, for a given average $\dot{\gamma}_{local}$, clusters grow undisturbed within the granule interstices when $d_{cluster} < d_G$, envelop granules if $d_{cluster} > d_G$, but interact with and are disrupted by granules of comparable size. For discontinuous shear thickening (DST) to occur, a cluster must span the entire system. While small clusters can form spontaneously in many regions of the suspension, the growth of larger clusters becomes increasingly constrained. Disruption of large clusters by large granules is particularly detrimental to the formation of force chains, thereby reducing the intensity of shear thickening. This explains the observed decrease in β_{max} with increasing granule size, as shown in Fig. 4(b).

In this scenario, where granules disrupt the force chains formed by the small particles depending on their relative size, granule density and surface interactions between small and large particles may also play a role. To probe this effect, a second DST suspension of fumed silica was prepared, to which 60 μm glass beads were added in different proportions. In addition to their distinct surface properties, the glass beads are significantly denser than PMMA, whose results for 60 μm spheres are presented in Fig. 3(a). The corresponding rheology curves with 60 μm glass beads are shown in Fig. 6(a). Once again, the addition of granules leads to a pronounced softening of the suspension, and a good data collapse was obtained at ϕ_G = 40% between the glass beads and the PMMA particles. Additionally, the surface of the 20 μm PS particles was modified to grow a thin glass coating using an adapted Stöber process.[40] The presence of silica on the granules was confirmed by energy dispersive spectroscopy (Ultim Max 100), see Fig. SM6 in the SI. In the same fumed silica suspension, and for the same granule volume fraction ϕ_G = 40%, the suspension rheology remained identical with and without the glass coating on the PS spheres, see Fig. 6(b). Taken together, these two additional series of experiments indicate that neither granule density nor surface chemistry need to be invoked to account for the observed softening. The disruption of clusters would then primarily depend on the granule volume fraction and on the size of the granules.

In other systems, the disruption of cluster growth, *i.e.*, the break-up of force chains, by ultrasound[41] or orthogonal oscillations[42] for instance, has been shown to inhibit the shear-thickening process. We hypothesize that, in the present case, the interaction and subsequent disruption of growing clusters by large granules are responsible for the observed size-dependent softening of shear thickening.

Conclusions

In experiments with various shear-thickening suspensions composed of small particles, we find that the addition of

 This journal is © The Royal Society of Chemistry 2026

Open Access Article. Published on 27 February 2026. Downloaded on 3/21/2026 5:15:28 AM.
This article is licensed under a Creative Commons Attribution 3.0 Unported Licence.

granules that are 20 to 120 times larger shifts the onset of thickening toward lower shear rates, leaves the onset shear stress nearly unchanged, and softens the shear thickening. This is in contrast with other systems discussed in prior literature, and we discuss the possible origins of the difference. The softening we observe, quantified by the maximum thickening index β_{max}, is robust across different systems: it persists when varying the nature of the small particles (varying in size from 500 nm to 2 μm, and from rough, non-spherical fumed silica to smooth silica spheres), the initial type of shear thickening (CST or DST) of the suspension in the absence of granules, as well as the granule size, density, and surface chemistry. Due to the large size contrast between granules and nanoparticles, any geometric effect should already be saturated and should be leading to identical effects for granules of different sizes. The granule size nevertheless plays a key role in determining the extent of this softening. To account for the observed softening in such highly bimodal suspensions, we propose that it is due to the interactions of the large granules with small-particle clusters, whose characteristic size increases with the applied stress. This tentative scenario could be confirmed with dedicated numerical studies or new experimental visualization techniques.

Safety and hazards

Dry fumed silica is easily aerosolized and extremely hazardous to the respiratory system, and must be handled with precautions inside a fume hood. See OSHA guidelines for detailed regulations.

Conflicts of interest

There are no conflicts to declare.

Data availability

Supplementary information (SI) is available. See DOI: https://doi.org/10.1039/d5sm01144b.

Data (rheology, SEM pictures), codes and scripts necessary to reproduce the results reported in this article are available at The Material Data Facility at DOI: https://doi.org/10.18126/tc7d-1e15.

Acknowledgements

We thank N. J. Wagner for useful discussion. This work was supported by the Army Research Office through grants W911NF-21-2-0146 and W911NF-25-2-0178. AP acknowledges the University of Chicago Materials Research Science and Engineering Center, funded by the National Science Foundation under award number DMR-2011854, for a Kadanoff-Rice Postdoctoral Fellowship.

Notes and references

1 R. Mari, R. Seto, J. F. Morris and M. M. Denn, *J. Rheol.*, 2014, **58**, 1693–1724.
2 J. F. Morris, *Annu. Rev. Fluid Mech.*, 2020, **52**, 121–144.
3 E. Brown and H. M. Jaeger, *Rep. Prog. Phys.*, 2014, **77**, 046602.
4 R. Hoffman, *J. Colloid Interface Sci.*, 1974, **46**, 491–506.
5 J. Lee, Z. Jiang, J. Wang, A. R. Sandy, S. Narayanan and X.-M. Lin, *Phys. Rev. Lett.*, 2018, **120**, 028002.
6 J. F. Brady and G. Bossis, *J. Fluid Mech.*, 1985, **155**, 105–129.
7 X. Cheng, J. H. McCoy, J. N. Israelachvili and I. Cohen, *Science*, 2011, **333**, 1276–1279.
8 R. Seto, R. Mari, J. F. Morris and M. M. Denn, *Phys. Rev. Lett.*, 2013, **111**, 218301.
9 M. van der Naald, L. Zhao, G. L. Jackson and H. M. Jaeger, *Soft Matter*, 2021, **17**, 3144–3152.
10 N. Fernandez, R. Mani, D. Rinaldi, D. Kadau, M. Mosquet, H. Lombois-Burger, J. Cayer-Barrioz, H. J. Herrmann, N. D. Spencer and L. Isa, *Phys. Rev. Lett.*, 2013, **111**, 108301.
11 J. R. Royer, D. L. Blair and S. D. Hudson, *Phys. Rev. Lett.*, 2016, **116**, 188301.
12 M. Wyart and M. E. Cates, *Phys. Rev. Lett.*, 2014, **112**, 098302.
13 C. Heussinger, *Phys. Rev. E:Stat., Nonlinear, Soft Matter Phys.*, 2013, **88**, 050201.
14 C. Clavaud, A. Bérut, B. Metzger and Y. Forterre, *Proc. Natl. Acad. Sci. U. S. A.*, 2017, **114**, 5147–5152.
15 E. Brown and H. M. Jaeger, *J. Rheol.*, 2012, **56**, 875–923.
16 C.-P. Hsu, S. N. Ramakrishna, M. Zanini, N. D. Spencer and L. Isa, *Proc. Natl. Acad. Sci. U. S. A.*, 2018, **115**, 5117–5122.
17 M. Blair and C. Ness, *J. Fluid Mech.*, 2022, **948**, A48.
18 S. R. Raghavan and S. A. Khan, *J. Colloid Interface Sci.*, 1997, **185**, 57–67.
19 P. Bourrianne, V. Niggel, G. Polly, T. Divoux and G. H. McKinley, *Phys. Rev. Res.*, 2022, **4**, 033062.
20 C. D. Cwalina and N. J. Wagner, *J. Rheol.*, 2014, **58**, 949–967.
21 R. Mari, R. Seto, J. F. Morris and M. M. Denn, *Proc. Natl. Acad. Sci. U. S. A.*, 2015, **112**, 15326–15330.
22 T. Kawasaki and L. Berthier, *Phys. Rev. E*, 2018, **98**, 012609.
23 É. Guazzelli and O. Pouliquen, *J. Fluid Mech.*, 2018, **852**, P1.
24 J. Chong, E. Christiansen and A. Baer, *J. Appl. Polym. Sci.*, 1971, **15**, 2007–2021.
25 S. Pednekar, J. Chun and J. F. Morris, *J. Rheol.*, 2018, **62**, 513–526.
26 F. Tapia, O. Pouliquen and É. Guazzelli, *Phys. Rev. Fluids*, 2019, **4**, 104302.
27 T. Stovall, F. De Larrard and M. Buil, *Powder Technol.*, 1986, **48**, 1–12.
28 A.-B. Yu and N. Standish, *Ind. Eng. Chem. Res.*, 1991, **30**, 1372–1385.
29 M. Sengun and R. Probstein, *Rheol. Acta*, 1989, **28**, 382–393.
30 S. Dagois-Bohy, S. Hormozi, É. Guazzelli and O. Pouliquen, *J. Fluid Mech.*, 2015, **776**, R2.
31 Y. Madraki, S. Hormozi, G. Ovarlez, E. Guazzelli and O. Pouliquen, *Phys. Rev. Fluids*, 2017, **2**, 033301.

Open Access Article. Published on 27 February 2026. Downloaded on 3/21/2026 5:15:28 AM.
This article is licensed under a Creative Commons Attribution 3.0 Unported Licence.

32 Y. Madraki, G. Ovarlez and S. Hormozi, *Phys. Rev. Lett.*, 2018, **121**, 108001.
33 C. D. Cwalina and N. J. Wagner, *J. Rheol.*, 2016, **60**, 47–59.
34 J. Bender and N. J. Wagner, *J. Rheol.*, 1996, **40**, 899–916.
35 A. Singh, C. Ness, A. K. Sharma, J. J. de Pablo and H. M. Jaeger, *Phys. Rev. E*, 2024, **110**, 034901.
36 B. J. Maranzano and N. J. Wagner, *J. Chem. Phys.*, 2001, **114**, 10514–10527.
37 B. M. Guy, M. Hermes and W. C. Poon, *Phys. Rev. Lett.*, 2015, **115**, 088304.
38 H. Kim, M. van der Naald, F. A. Braaten, T. A. Witten, S. J. Rowan and H. M. Jaeger, *Soft Matter*, 2024, **20**, 6384–6389.
39 N. Malbranche, B. Chakraborty and J. F. Morris, *J. Rheol.*, 2023, **67**, 91–104.
40 C. Graf, D. L. Vossen, A. Imhof and A. van Blaaderen, *Langmuir*, 2003, **19**, 6693–6700.
41 P. Sehgal, M. Ramaswamy, I. Cohen and B. J. Kirby, *Phys. Rev. Lett.*, 2019, **123**, 128001.
42 N. Y. Lin, C. Ness, M. E. Cates, J. Sun and I. Cohen, *Proc. Natl. Acad. Sci. U. S. A.*, 2016, **113**, 10774–10778.

 This journal is © The Royal Society of Chemistry 2026